Ceramics International 46 (2020) 4947–4951

Contents lists available at ScienceDirect

Ceramics International

journal homepage: www.elsevier.com/locate/ceramint

Production and properties of phase separated porous glass

E. Burak Ertuş[a,b], Cekdar Vakifahmetoglu[c,*], Abdullah Öztürk[a]

[a] Middle East Technical University, Department of Metallurgical and Materials Engineering, Ankara, Turkey
[b] KTO Karatay University, Department of Metallurgical and Materials Engineering, Konya, Turkey
[c] İzmir Institute of Technology, Department of Materials Science and Engineering, İzmir, Turkey

ARTICLE INFO

Keywords:
Sodium borosilicate glass
Porous glass
Phase separation
Leaching
Wear

ABSTRACT

A sodium borosilicate glass (SBG) was produced by conventional melt-quenching. As cast glass was heat treated to induce phase separation (SBG-HT), followed by acid leaching with HCl to dissolve one of the separated phases; i.e. alkali rich borate phase, so that a porous glass (PG) was obtained. In order to alter the pore structure, produced PG was subsequently alkali (NaOH) leached or alternatively heat treated. The samples were characterized by techniques including XRD, SEM, N_2 adsorption/desorption. The total pore volume for PG was found to be 0.314 cm^3/g, reached to 0.370 cm^3/g by alkali leaching, instead decreased to 0.227 cm^3/g by heat treatment. The microhardness and tribological properties of SBG-HT and all PGs were evaluated by Vickers hardness and by pin on disk tribometer. For all PGs the microhardness values were lower, instead the wear rates were higher than that of the parent SBG-HT.

1. Introduction

In recent years, porous glasses (PGs) have received considerable attention because of their unique properties. PGs can be prepared by several different ways such as sacrificial templating, partial sintering, high temperature bonding, blowing agents, sol-gel, etc. [1–3]. In order to produce high surface area, permeable glass components, phase separated glasses can be leached to extract one of the separated phases. This is actually an intermediate step of *Vycor* process in which an alkali borosilicate glass is exposed to *spinodal decomposition* (i.e. phase separation) followed by selective leaching of alkali-borate phase by aqueous acidic solutions [4,5]. The resultant amorphous porous material with high silica (SiO_x) content (~96 wt%) could further be processed by alkali treatment followed by sintering to obtain highly dense glass products [5]. If the component interested is porous, its pore size can be altered in a broad range from 0.3 to 1000 nm with a surface area reaching ~340 m^2/g [6] by changing the processing conditions such as initial batch composition, heat treatment, and following leaching procedures [7].

Sodium borosilicate is the most commonly studied glass family that can be phase separated by a regulated heat treatment to silicate and borate rich (alkali-borate) phases. These phases can actually be designed to form three-dimensionally entangled, continuous, split networks in the same glass matrix. During the phase separation, certain amount of silicate phase remains dissolved in the alkali-borate phase. However, still what is so called *liquation channels* are formed when alkali-borate rich phase is leached out by aqueous acidic solutions, generating interconnected, open-pore structure in the remaining silicate matrix. The silicate domains/regions of the dissolved alkali-borate phase may remain in the leaching solution as colloidal silica, coagulating to form silica clusters that cannot be dissolved in the acidic solution [6,8,9]. Accordingly, hierarchically porous artifacts with pore sizes around 7–54 nm due to liquation channels (interconnected network) [6,8], and around 2–5 nm due to spaces in between silica clusters (and the gaps that is in between those with channel walls) [6,8,9] together with intra-particle porosity (0.4–0.7 nm) [10,11] are generally observed. The silica clusters remaining inside the channels can be removed by basic (alkaline) solutions which may further enlarge the channel diameter as well [12]. If the final material is successively heat treated (e.g. at 900 °C for < 70 h) [13], viscous flow sintering leads consolidation. This procedure can also be used to design the final pore architecture [14–16].

Depending on the pore size, PGs may exhibit optical transparency, decent mechanical stability, and high chemical resistance to most organic solvents and acids (except HF) [13]. The porous components could be used as membrane, optical chemo-sensor and drug delivery system with a wide variety of geometric forms such as beads, fibers, and monoliths [5,7].

Compared to other techniques, creating porosity by phase separation and acid leaching is commonly practiced because it is rather easy

* Corresponding author.
E-mail addresses: cekdarvakifahmetoglu@iyte.edu.tr, cvahmetoglu@gmail.com (C. Vakifahmetoglu).

https://doi.org/10.1016/j.ceramint.2019.10.232
Received 15 September 2019; Received in revised form 21 October 2019; Accepted 24 October 2019
Available online 24 October 2019
0272-8842/ © 2019 Elsevier Ltd and Techna Group S.r.l. All rights reserved.

to control the pore topology and it suits better for low cost, mass production. However, stress development particularly during leaching step is a major problem and mechanically stable, crack free components are difficult to obtain [17,18]. Studies reporting the mechanical and structural properties of PGs are very limited [19–21], in fact there is no systematic study on the wear behavior of PGs. Understanding the mechanical and tribological behavior of PG could extend its utilization in applications. Accordingly, this work aims to produce phase separated sodium borosilicate glass (SBG-HT), followed by leaching to obtain different types of PGs. Hardness and tribological properties of the formed samples are evaluated and compared with that of the parent non-porous SBG-HT.

2. Experimental procedure

2.1. Sample preparation

Reagent grade Na_2CO_3 (Merck), H_3BO_3 (Eti Maden), $Al(OH)_3$ (Eti Alüminyum) and SiO_2 (Eczacıbaşı) powders were used in appropriate amounts to yield a glass with nominal composition of $55.7SiO_2$-$33.6B_2O_3$-$9.2Na_2O$-$1.5Al_2O_3$ (wt. %) by a conventional melt-quenching. First, the powders were mixed in an agate mortar with pestle to produce a homogeneous mixture ~42 g. The batch then was put in a 90 Pt–10Rh crucible and placed in an electrically heated furnace (atmospheric, PT1700 M, China) for melting at 1300 °C at the heating rate of 10 °C/min, and kept at the peak temperature for 2 h. The melts were quenched in air and the resulting glass shards were further crushed and re-melted at 1400 °C for 2 h to ensure chemical homogeneity and to get a readily castable melt. After that, the melt was re-quenched onto a stainless-steel plate at room temperature (RT) and another steel plate weighing 1 kg (causing an approximate pressure of 0.001 MPa) was placed on the melt (with no additional pressure) to obtain a flat surface while solidification proceeding.

The glass pieces (SBG) were heat treated at 500 °C for 9 h to induce the phase separation (SBG-HT). Then, they were cut to ~2 cm square shaped specimens. A thin protective silica rich layer formed due to volatilization of sodium and borate during heat treatment [4] was removed by mechanical polishing using 3 μm diamond paste finish. The final thickness of the specimens was about 2 ± 0.1 mm.

In order to prepare porous glasses (PGs), parent sodium borosilicate glass (SBG-HT) was first acid treated using 1 M HCl solution at 80 °C for 24 h. The acid treated PG was then washed with distilled water and ethanol repeatedly, and dried at 90 °C for 3 h in an oven. In order to remove silica clusters (those already dissolved in borate-rich phase) remained in the liquation channels of acid leached glass matrix, an additional alkali treatment was followed by using 0.5 M NaOH solution for 2 h at RT. The alkali treated PG was coded as PG-AL. Apart from the PG-AL, by heat treating the PG at 800 °C for 1 h, heat treated PG, i.e. PG-HT, was produced. PGs with various pore size and shape were produced through these treatments to find out a correlation between the pore architecture and the resulting properties.

2.2. Characterization

Glassiness of all samples (SBG, SBG-HT, PG, PG-AL, and PG-HT) was investigated using an X-ray diffractometer (Bruker-AXS, D8 Advance A25). The diffraction patterns were taken between 2θ of 10° and 90° at a scanning rate of 2°/min and step size of 0.02° using Cu-K_α radiation. Pore characteristics were evaluated by N_2 sorption by using Quantachrome Autosorb-6 (Florida, USA). The specific surface area (SSA) was calculated by using Brunauer–Emmett–Teller (BET) equation. The total pore volume (V_P) was found from the amount of gas adsorbed at the relative pressure $P/P_0 = 0.99$. The pore size distributions were determined from the desorption branch of the N_2 sorption isotherm according to the BJH (Barrett, Joyner, Halenda) method [22]. The bulk density (ρ_b) and open porosity (V_o) values were measured by the Archimedes method using water as buoyancy fluid in accordance with ASTM B962-15 and ASTM C373-18 standards taking the density of water at 25 °C as 0.99 g/cm^3 [23,24].

The Vickers hardness (H_V) values, average of 15 indents, was measured using microhardness tester (Shimadzu, HSV-20) merely by applying 500 g load for 10 s. Tribological tests were performed using a pin-on-disc tribometer (CSM Instruments, Massachusetts, USA) in accordance with ASTM G99- 95A standard [25]. 1 N and 5 N loads were applied at 100 Hz rate at 0.03 m/s linear speed. The sliding distance was 60 m and application radius was 3 mm for each test. A high purity zirconia ball of 1.5 mm radius was employed as a pin material and was replaced after each test. No significant pin wear was detected after an individual test. The wear tests were repeated five times to assure the reproducibility of the data. The surface profile of the worn specimens was measured using a stylus profilometer (Mitutoyo Surftest SJ-400, Illinois, USA) to determine the worn track depth and worn area. The wear rate was calculated by using Equation (1).

$$W = \frac{V}{P.\,L} \tag{1}$$

where; W is the wear rate in mm^3/N.m, V is the calculated volume loss in mm^3, P is the normal load in N, and L is the sliding distance in m. The wear tracks were subsequently analyzed using a scanning electron microscope (FESEM, Nova Nanosem 430, Oregon ABD). Prior to SEM examinations specimen surfaces were coated with ≅10 nm layer of gold by a sputter coater (Quorum SC7640, United Kingdom).

3. Results and discussion

XRD patterns of SBG, SBG-HT, PG, PG-AL, and PG-HT shown in Fig. 1 demonstrate the presence silica/silicate related halo in between 15 and 30° (2θ). In other words, devitrification was not detected for all samples. The fingerprint of spinodal decomposition at ~45° (2θ) seen in SBG-HT glass [26,27], diminished upon acid leaching, akin to the results reported by Lee et al. [28].

N_2 sorption isotherms of SBG-HT, PG, PG-AL, and PG-HT are given in Fig. 2(a). While permeability tests were not applied on the samples, the sorption data demonstrates that all PGs have 3D interconnected porosity with Type IVa isotherm according to the IUPAC classifications [29]. The capillary condensation is accompanied by hysteresis and the glasses exhibit combination of H2a and H2b type of hysteresis which is generally related with pore-blocking/percolation in a narrow range of pore necks or cavitation-induced evaporation [29]. The pore size distribution curves, shown in Fig. 2(b), demonstrate that the samples have hierarchical porosity. The pores centered in the range of 3–5 nm are

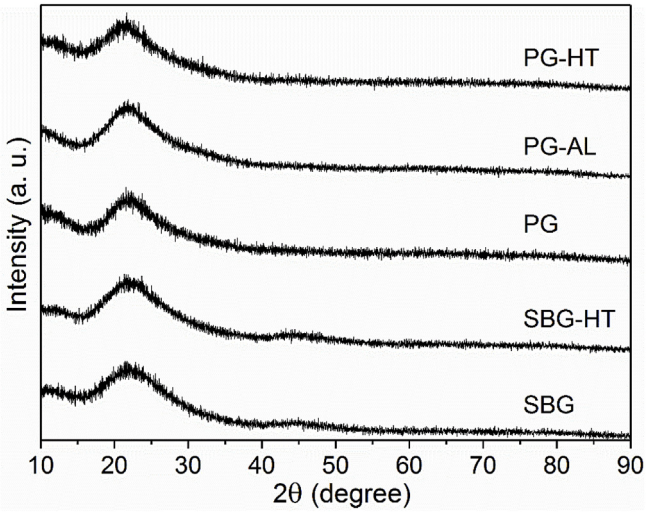

Fig. 1. XRD patterns of the SBG, SBG-HT, PG, PG-AL, and PG-HT.

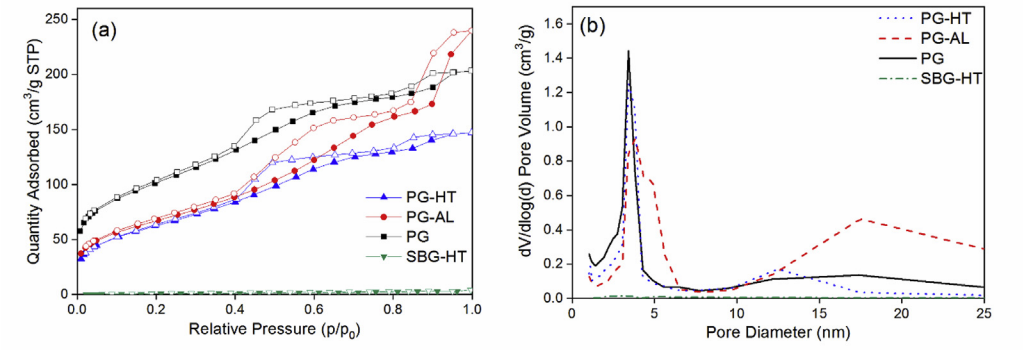

Fig. 2. (a) N_2 adsorption-desorption isotherms, and **(b)** pore size distribution curves of SBG-HT, PG, PG-AL, and PG-HT.

Table 1
Pore characteristics, bulk density, microhardness, and tribological properties of SBG-HT, PG, PG-AL, and PG-HT.

Sample	SSA (m^2/g)	V_P (cm^3/g)	ρ_b (g/cm^3)	V_O (%)	Hv (MPa)	W (× $10^{-4}$$mm^3$/Nm)		μ mean	
						1 N	5 N	1 N	5 N
SBG-HT	3.5	0.006	2.23	0	4296	1.06	2.73	0.80	0.79
PG	358.0	0.314	1.35	36	298	11.82	26.02	0.47	0.50
PG-AL	241.2	0.370	1.25	41	79	90.19	135.47	0.41	0.49
PG-HT	228.4	0.227	1.52	30	332	11.91	23.83	0.49	0.48

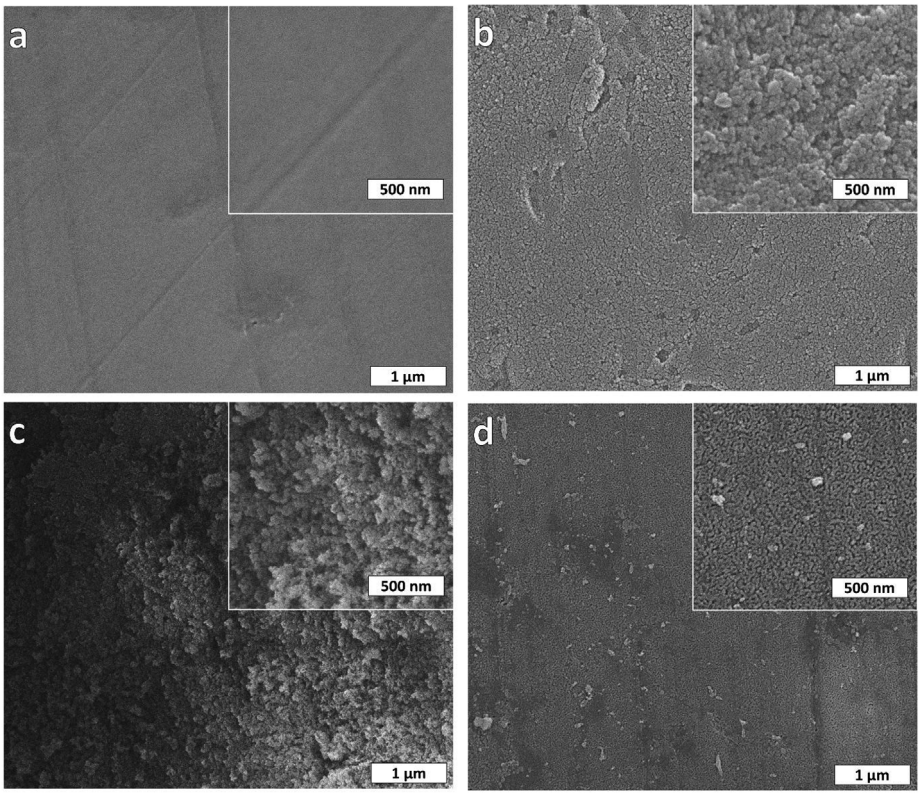

Fig. 3. SEM micrographs taken from the fracture surfaces of **(a)** SBG-HT, **(b)** PG, **(c)** PG-AL, and **(d)** PG-HT. Insets are larger magnification of the images.

associated to inter-particle spaces in between the channel walls and silica clusters (themselves as well). Instead relatively larger mesopores evolved in a broader range from 7 to 35 nm are due to the so called *liquation channels* [9,10]. It is important to note that all curves resemble those seen in previous studies [10,11].

When successive alkaline treatment was conducted on the PGs, the size of the pores in the mesopore range (2–50 nm) increased but micropores diminished to some extent. Probably this is due to particle and/or surface dissolution of silica clusters [30] resulting in the reduction of SSA but enhancement in the pore volume. Instead, when PG was additionally heat treated viscous flow caused contraction for all types of pores and eventually both SSA and pore volume decreased as could be seen also in Table 1.

As a result of the acid leaching process, the bulk density of parent SBG-HT decreased from 2.23 to 1.35 g/cm^3 and the PG had an open porosity around 36 vol%, comparable to previous reports [13,15,20].

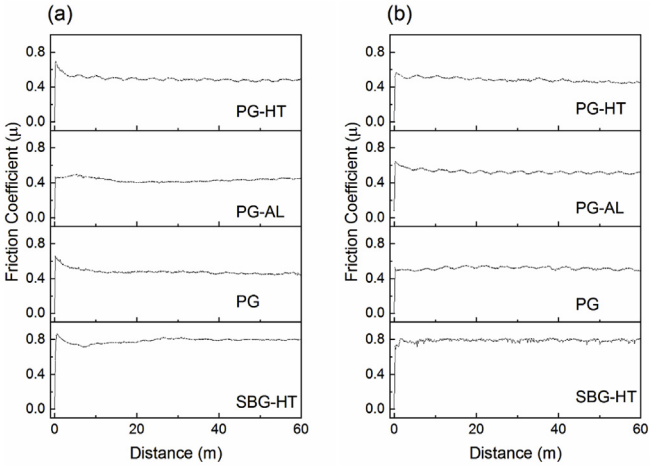

Fig. 4. Variation in the friction coefficient with sliding distance at a load of **(a)** 1 N and **(b)** 5 N.

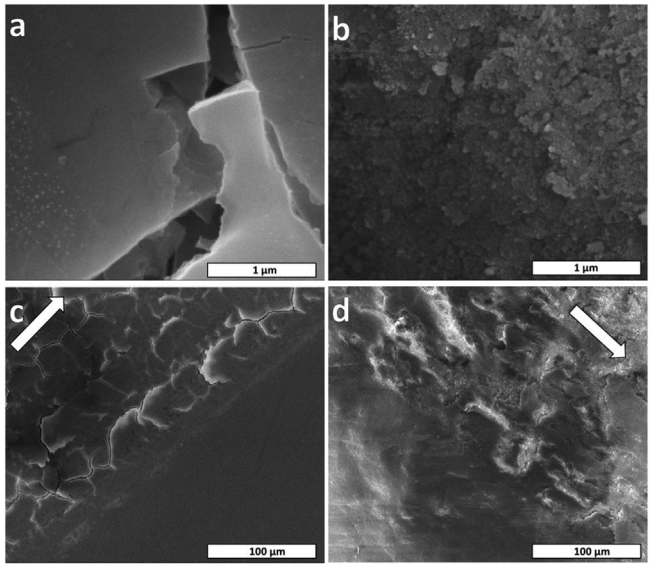

Fig. 5. SEM images of wear tracks at 1 N load which were taken from the center of **(a)** SBG-HT, and **(b)** PG. Magnified images taken from the edge to show wear tracks for **(c)** SBG-HT, and **(d)** PG.

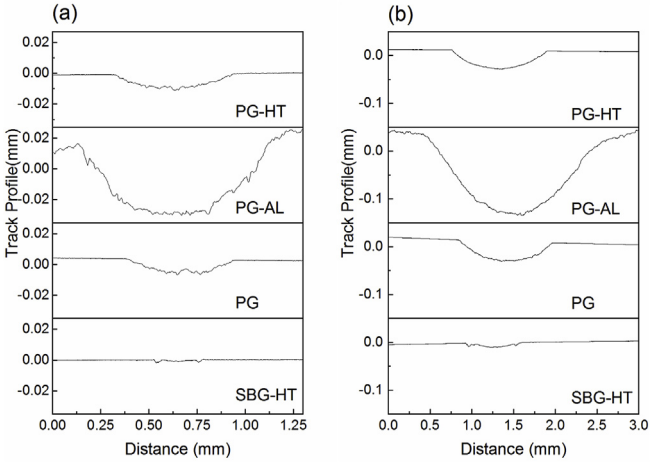

Fig. 6. Wear track profiles at a load of **(a)** 1 N and **(b)** 5 N.

The bulk density of PG-HT was higher than that of the PG indicating a densification during the heat treatment.

Fig. 3 shows the SEM images taken from the surface of the SBG-HT, PG, PG-AL, and PG-HT. Characteristic “worm-like” porous structure formed after acid leaching process analogous to what was reported [7,31]. As compared to PG, alkaline treatment caused a deformation in the microstructure, though heat treatment resulted in a densification.

It is rather difficult to speculate on the hardness results since generally speaking the mechanical properties of PGs have not been covered well in the literature, and certainly further studies are needed. Concerning the samples in this study; as given in Table 1, hardness of PG is considerably lower than that of SBG-HT. Excluding the effect of indentation load which was not examined in the study (note that the applied load is higher than 100 gf [32]). The decline in hardness might be attributed to two reasons. First, the thin pore walls cannot withstand the highly localized pressure of the indenter and fracture. Second, the porosity prevents elastic recovery of the indents due to huge free volume in the indented area [33]. As a result of heat treatment, an enhancement in the hardness was observed due to partial sintering although the sample was still highly porous and still prone to indentation failure compared to parent SBG-HT. Along the same line, Scherer et al. [34] showed that the Young's modulus of porous glass increased by successive heat treatments but the micro cracks formed during acid leaching could not be healed.

Friction coefficient (μ) and wear rate (W) values of the glasses are also given in Table 1. Typically, W of PG is about ten times bigger than that of SBG-HT both under 1 N and 5 N loads, implying that the thin pore walls can easily be broken [35]. When alkaline treatment was conducted, as expected, generation of additional residual etching stresses and porosity (0.314 vs. 0.370 g/cm^3 pore volume) caused an increase of W for PG-AL compared to PG under all loads. On the other hand, successive heat treatment had no significant effect on W.

The variation in μ with sliding distance under loads of 1 N and 5 N is shown in Fig. 4 (a and b). It is clear that the μ of all porous glasses was lower than that of the SBG-HT. This finding is consistent with previous reports in which it was stated that porous and textured surfaces act as a lubricant reservoir and reduce friction coefficient [36,37]. Further experiments are necessary to elucidate these findings but PG is also a good moisture absorber [38]. The water molecules bound in the glass skeleton may play a lubricating role and/or fine wear debris may act as a self-lubricating character.

SEM images of wear tracks for SBG-HT and PG are given in Fig. 5. The white arrows in the SEM images indicate the sliding direction of the counterface. For SBG-HT, there are clear cracks with the sizes ranging from 10 to 40 μm. The cracks spread from the edge to the outside of the wear track. Instead for PG, such large flaws did not occur due probably to the nano-sized pores preventing the crack propagation. The debris formed during friction was accumulated and a debris layer was formed on the worn surface. The area of these layers was found to be larger for SBG-HT as compared to that for PG.

The wear surface of SBG-HT is smoother than that of all porous glasses. See wear track profiles shown in Fig. 6 **(a** and **b)** corroborating further a higher μ value for parent SBG-HT compared to that for porous samples [39]. Since the hardness values were much lower than that of the zirconia ball counterface, all the surface layers were worn away significantly due to mechanical abrasion and brittle failure [40,41].

4. Conclusions

Hierarchically porous glasses (PGs) having moderately high specific surface area (358 m^2/g) were produced by acid leaching process conducted on a sodium borosilicate glass with a nominal composition of $55.7SiO_2$-$33.6B_2O_3$-$9.2Na_2O$-$1.5Al_2O_3$ (wt.%). The acid and successive alkaline treatments have profound effects on the pore structure, microhardness, and tribological properties of the PG. While the hardness (298 MPa) and friction coefficient (0.47) of the PG was lower, the wear

rate (11.82×10^{-4} mm^3/N.m at 1 N load) was higher to that of the SBG-HT due to the generation of residual etching stresses and additional porosity. The total pore volume and wear rate further increased with successive alkaline treatment (PG-AL) and the microhardness decreased. Instead, the heat treatment conducted on PG did not have a significant effect on the microhardness and the wear rate.

Acknowledgments

The authors thank Middle East Technical University (METU, Ankara, Turkey) for the partial financial support through project (BAP-03-08-2016-004). The authors also thank to METU central laboratory for N_2 sorption tests.

References

[1] A.M.M. Santos, W.L. Vasconcelos, Properties of porous silica glasses prepared via sol–gel process, J. Non-Cryst. Solids 273 (2000) 145–149.
[2] E.C. Bucharsky, K.G. Schell, R. Oberacker, M.J. Hoffmann, Preparation of transparent glass sponges via replica method using high-purity silica, J. Am. Ceram. Soc. 93 (2010) 111–114.
[3] A. Sadighzadeh, M. Ghoranneviss, A.S. Elahi, Application of partial sintering of waste glasses for preparation of porous glass bodies, J. Porous Mater. 21 (2014) 993–999.
[4] H.H. Porter, N.M. Emery, Treated Borosilicate Glass, Google Patents, 1938.
[5] T.H. Elmer, Porous and reconstructed glasses, ASM Int., Eng. Mater. Handbook 4 (1991) 427–432.
[6] D. Enke, K. Otto, F. Janowski, W. Heyer, W. Schwieger, W. Gille, Two-phase porous silica: mesopores inside controlled pore glasses, J. Mater. Sci. 36 (2001) 2349–2357.
[7] D. Enke, F. Janowski, W. Schwieger, Porous glasses in the 21st century—a short review, Microporous Mesoporous Mater. 60 (2003) 19–30.
[8] D. Enke, F. Janowski, W. Gille, W. Schwieger, Structure and texture analysis of colloidal silica in porous glasses, Colloid. Surf. Physicochem. Eng. Asp. 187 (2001) 131–139.
[9] G. Toquer, C. Delchet, M. Nemec, A. Grandjean, Effect of leaching concentration and time on the morphology of pores in porous glasses, J. Non-Cryst. Solids 357 (2011) 1552–1557.
[10] V. Kreisberg, V. Rakcheev, T. Antropova, Influence of the acid concentration on the morphology of micropores and mesopores in porous glasses, Glass Phys. Chem. 32 (2006) 615–622.
[11] V. Kreisberg, V. Rakcheev, T. Antropova, Microporosity of porous glasses: new investigation techniques, Glass Phys. Chem. 29 (2003) 541–547.
[12] W. Haller, Rearrangement kinetics of the liquid—liquid immiscible microphases in alkali borosilicate melts, J. Chem. Phys. 42 (1965) 686–693.
[13] M.E. Nordberg, Properties of some Vycor-brand glasses, J. Am. Ceram. Soc. 27 (1944) 299–305.
[14] S. Stolyar, T. Antropova, D. Petrov, I. Anfimova, Viscosity and shrinkage of porous and quartzoid glasses of the Na_2O-B_2O_3-SiO_2 system, Russ. J. Appl. Chem. 81 (2008) 974–977.
[15] T. Antropova, I. Drozdova, T. Vasilevskaya, A. Volkova, L. Ermakova, M. Sidorova, Structural transformations in thermally modified porous glasses, Glass Phys. Chem. 33 (2007) 109–121.
[16] A. Volkova, L. Ermakova, M. Sidorova, T. Antropova, I. Drozdova, The effect of thermal treatment on the structural and electrokinetic properties of porous glass membranes, Colloid J. 67 (2005) 263–270.
[17] G.W. Scherer, M.G. Drexhage, Stress in leached phase-separated glass, J. Am. Ceram. Soc. 68 (1985) 419–426.
[18] H.P. Hood, M.E. Nordberg, Method of Treating Borosilicate Glasses, Google Patents, 1942.
[19] B. Reinhardt, D. Enke, F. Syrowatka, Preparation of porous, hierarchically organized glass monoliths via combination of sintering and phase separation, J. Am. Ceram. Soc. 95 (2012) 461–465.
[20] D. O'Brien, T. Juliano, P. Patel, S. McKnight, Optically Transparent Nanoporous Glasspolymer Composites, Army Research Lab., 2006.
[21] T. Aytug, J.T. Simpson, A.R. Lupini, R.M. Trejo, G.E. Jellison, I.N. Ivanov, S.J. Pennycook, D.A. Hillesheim, K.O. Winter, D.K. Christen, Optically transparent, mechanically durable, nanostructured superhydrophobic surfaces enabled by spinodally phase-separated glass thin films, Nanotechnology 24 (2013) 315602.
[22] L.G. Joyner, E.P. Barrett, R. Skold, The determination of pore volume and area distributions in porous substances. II. Comparison between nitrogen isotherm and mercury porosimeter methods, J. Am. Chem. Soc. 73 (1951) 3155–3158.
[23] ASTM, Standard Test Method for Water Absorption, Bulk Density, Apparent Porosity and Apparent Specific Gravity of Fired Whiteware Products" C3vols. 73–88 ASTM International, West Conshohocken, PA, 2006.
[24] ASTM, Standard Test Methods for Density of Compacted or Sintered Powder Metallurgy (PM) Products Using Archimedes' Principle, B962-13, ASTM International, West Conshohocken, PA, 2013.
[25] ASTM, Standard Test Method for Wear Testing with a Pin-On-Disk Apparatus G99 ASTM International, West Conshohocken, PA, 2010, pp. 1–5.
[26] J. Kim, S. Lee, D. Shin, Preparation of a hybrid solid glass electrolyte using a nanoporous sodium borosilicate glass membrane for lithium batteries, J. Ceram. Process. Res. 8 (2007) 208.
[27] D.R. Patwari, B. Eraiah, Luminescence properties of erbium doped sodium barium borate glass with silver nanoparticles, IOP Conference Series: Materials Science and Engineering, IOP Publishing, 2018012056.
[28] S.H. Lee, K.I. Cho, J.B. Choi, D.W. Shin, Phase separation and electrical conductivity of lithium borosilicate glasses for potential thin film solid electrolytes, J. Power Sources 162 (2006) 1341–1345.
[29] M. Thommes, K. Kaneko, A.V. Neimark, J.P. Olivier, F. Rodriguez-Reinoso, J. Rouquerol, K.S. Sing, Physisorption of gases, with special reference to the evaluation of surface area and pore size distribution (IUPAC Technical Report), Pure Appl. Chem. 87 (2015) 1051–1069.
[30] M. Lyubavin, T. Burkat, V. Pak, Fabrication of silica membranes with controlled pore structure, Inorg. Mater. 44 (2008) 203–206.
[31] T. Elmer, M. Nordberg, G. Carrier, E. Korda, Phase separation in borosilicate glasses as seen by electron microscopy and scanning electron microscopy, J. Am. Ceram. Soc. 53 (1970) 171–175.
[32] E. Broitman, Indentation hardness measurements at macro-, micro-, and nanoscale: a critical overview, Tribol. Lett. 65 (2017) 23.
[33] W. Lo, A. Campbell, J. Luo, R. Stevens, Indentation-induced deformation and microcracking of highly textured superconducting $(Bi,Pb)_2$ $Sr_2Ca_2Cu_3O_X$ ceramic, J. Mater. Res. 10 (1995) 568–577.
[34] G.W. Scherer, Dilatation of porous glass, J. Am. Ceram. Soc. 69 (1986) 473–480.
[35] G. Lu, G.M. Lu, Z. Xiao, Mechanical properties of porous materials, J. Porous Mater. 6 (1999) 359–368.
[36] Z. Pawlak, W. Urbaniak, T. Kaldonski, A. Oloyede, Importance of Bearing Porosity in Engineering and Natural Lubrication, Biomaterials and Medical Tribology, Elsevier, 2013, pp. 311–354.
[37] M. Wakuda, Y. Yamauchi, S. Kanzaki, Y. Yasuda, Effect of surface texturing on friction reduction between ceramic and steel materials under lubricated sliding contact, Wear 254 (2003) 356–363.
[38] K. Hokkirigawa, T. Okabe, K. Saito, Friction properties of new porous carbon materials: woodceramics, J. Porous Mater. 2 (1996) 237–243.
[39] D. Mondal, S. Das, N. Jha, Dry sliding wear behaviour of aluminum syntactic foam, Mater. Des. 30 (2009) 2563–2568.
[40] G. Stachowiak, A.W. Batchelor, Engineering Tribology, Butterworth-Heinemann, 2013, pp. 483–500.
[41] H. He, L. Qian, C.G. Pantano, S.H. Kim, Mechanochemical wear of soda lime silica glass in humid environments, J. Am. Ceram. Soc. 97 (2014) 2061–2068.